

# Tracking interactions between TAMs and CAFs mediated by arginase-induced proline production during immune evasion of HCC

Bo Tang<sup>1</sup>, Chuanchen Wu<sup>1</sup>, Yuantao Mao<sup>1</sup>, Xinru Qi<sup>1</sup>, Xin Wang<sup>1</sup>, Ping Li<sup>1</sup>, and Wen Zhang<sup>1</sup>

<sup>1</sup>Shandong Normal University School of Chemistry Chemical Engineering and Materials

March 24, 2024

## Abstract

Synergistic changes between tumor-associated macrophages (TAMs) and tumor-associated fibroblasts (CAF) aggravated immune evasion of hepatocellular carcinoma (HCC), however, the underlying molecular mechanisms remain elusive. Their continuous and dynamic interactions are subject to bioactive molecule changes. A real-time and in-situ monitoring method suitable for in vivo research of these processes would be indispensable but is scarce. In this study, a dual imaging strategy that tracing the TAMs and CAFs simultaneously was developed using a new arginase-specific probe and established CAFs-specific probe. The emerging roles of arginase in mediating CAFs activation in mice were explored. Results showed arginase up-regulation in TAMs, followed by proline increase. Subsequently, proline produced by TAMs initiated the activation of CAFs. Through the JAK-STAT signaling, CAFs up-regulated the PD-L1 and CTLA-4, ultimately promoting immune evasion of HCC. This study revealed a new mechanism by which TAMs and CAFs collaborate in immune evasion, providing new targets for HCC immunotherapy.

Tracking interactions between TAMs and CAFs mediated by arginase-induced proline production during immune evasion of HCC

Chuanchen Wu, Yuantao Mao, Xinru Qi, Xin Wang, Ping Li, \*Wen Zhang and Bo Tang\*

C. C. Wu, Y. T. Mao, X. R. Qi, X. Wang, Prof. P. Li, W. Zhang and Prof. B. Tang

College of Chemistry, Chemical Engineering and Materials Science, Collaborative Innovation Center of Functionalized Probes for Chemical Imaging in Universities of Shandong, Key Laboratory of Molecular and Nano Probes, Key Laboratory of Molecular and Nano Probes, Ministry of Education, Institutes of Biomedical Sciences

Shandong Normal University

Jinan 250014, People's Republic of China

mail: lip@sdnu.edu.cn, tangb@sdnu.edu.cn

Prof. B. Tang

Laoshan Laboratory

168Wenhai Middle Rd, Aoshanwei Jimo

Qingdao 266237, People's Republic of China

E-mail: tangb@sdnu.edu.cn

**Keywords:** Fluorescent probe, Arginase, Tumor-associated macrophages, Immune evasion, Tumor-associated fibroblasts

**Abstract:** Synergistic changes between tumor-associated macrophages (TAMs) and tumor-associated fibroblasts (CAFs) aggravated immune evasion of hepatocellular carcinoma (HCC), however, the underlying molecular mechanisms remain elusive. Their continuous and dynamic interactions are subject to bioactive molecule changes. A real-time and in-situ monitoring method suitable for in vivo research of these processes would be indispensable but is scarce. In this study, a dual imaging strategy that tracing the TAMs and CAFs simultaneously was developed using a new arginase-specific probe and established CAFs-specific probe. The emerging roles of arginase in mediating CAFs activation in mice were explored. Results showed arginase up-regulation in TAMs, followed by proline increase. Subsequently, proline produced by TAMs initiated the activation of CAFs. Through the JAK-STAT signaling, CAFs up-regulated the PD-L1 and CTLA-4, ultimately promoting immune evasion of HCC. This study revealed a new mechanism by which TAMs and CAFs collaborate in immune evasion, providing new targets for HCC immunotherapy.

## 1. Introduction

Immune evasion of hepatocellular carcinoma (HCC) adopts multiple mechanisms to prevent antigen presentation, evade immune surveillance and clearance, promoting the continuous proliferation and further metastasis of HCC<sup>[1]</sup>. This is one of the essential characteristics of HCC progression. Importantly, immune evasion is a crucial reason for patients' resistance to immunotherapy drugs for HCC<sup>[2]</sup>. Immune evasion poses enormous challenges for patients' treatment and leads to a high mortality rate of HCC. Exploring the process of HCC immune evasion and revealing its related molecular mechanisms is pivotal to the development of more effective HCC treatment methods<sup>[3]</sup>.

The tumor microenvironment (TME) is the pathological environment in which immune evasion of HCC progression occurs<sup>[4]</sup>. The intercellular communication in TME is vital pathway for immune evasion<sup>[5]</sup>. To reveal the detailed molecular mechanisms of HCC immune evasion, it is prerequisite to explore the interplay of cells inside TME. Tumor-associated macrophages (TAMs) and tumor-associated fibroblasts (CAFs) are essential members of TME and exhibit various immunosuppressive functions<sup>[6]</sup>. Importantly, their mutual interactions in TME can induce recruitment and activation of each other, further enhancing immune evasion<sup>[7]</sup>. Although studies have reported the importance of CAFs and TAMs in tumor progression, the intercellular interaction mechanisms between them have not been fully revealed. Especially during the process of HCC immune evasion, the synergistic effect of CAFs and TAMs yet to be explored, and the detailed molecular mechanism remains elusive.

Arginase is a highly active enzyme that mostly expressed in TAMs<sup>[8]</sup>. Arginase consumes arginine in the TME, leading to T cell exhaustion, thus plays crucial roles in TAMs-mediated immune evasion<sup>[9]</sup>. In addition, arginase participates in regulating downstream pathways for the extracellular matrix (ECM) generation in the TME<sup>[10]</sup>. CAFs are responsible for ECM generation in the TME<sup>[11]</sup>. These findings suggest a hypothesis that TAMs might regulate the activity of CAFs through arginase, thereby affecting immune evasion of HCC. However, the underlying molecular mechanisms are mysterious. Cellular interplay between CAFs and TAMs is a continuous and dynamic process that is regulated by multiple active molecules. However, commonly used in vitro characterization methods such as western blot and polymerase chain reaction (PCR) are insufficient to explore the changes of active molecules in the physiological environment. The continuous and dynamic changes of arginase during the interaction between TAMs and CAFs are unrevealed. Fluorescence imaging technique would be a powerful tool for revealing the real-time and in-situ changes of arginase in the interaction between TAMs and CAFs in vivo, but applicative imaging strategy is lacking<sup>[12]</sup>.

Therefore, in this study, we have developed a dual imaging strategy that tracing the dynamic changes of TAMs and CAFs in cells and HCC mice. To fulfil this goal, a new fluorescent probe TPEARARG which emits bright fluorescence upon targeting arginase was constructed. This method enables in-situ dynamic imaging of arginase changes in TAMs. By combining this imaging strategy with our established CAFs activation-specific imaging method, we have investigated the dynamic role of TAMs-derived arginase in promoting

CAFs activation and facilitating immune evasion of HCC. The experimental results demonstrate that as the level of arginase in TAMs rises, the content of proline significantly increases. We have observed that the increased content of proline can significantly enhance the activation level of CAFs, which in turn affects the JAK-STAT pathway and enhances immune evasion of HCC.

## 2. Result

### 2.1. Design strategy of TPEARARG and optical properties of TPEARARG

Rational selection of identifying group, regulation mechanism of fluorescence and appropriate fluorophore were made to fabric the fluorescent probe that fulfill our demand. Firstly, knowing that the active site domain of arginase was specific to arginine, thus we chose arginine as the identifying group<sup>[8a]</sup>. Then, according to the steric hindrance change after the probe bound to the active site domain of the arginase, aggregation-induced emission (AIE) principle was selected as the fluorescence regulation mechanism after recognition<sup>[13]</sup>. Tetraphenylethene (TPE) is an excellent AIE fluorophore with outstanding fluorescence imaging performance. TPE structure is compact with low steric hindrance, which is conducive to the probe entering the ectodomain of enzyme, so as to achieve high specificity and high selectivity imaging detection of enzymes<sup>[14]</sup>. In light of these considerations, we incorporated an arginine moiety to a TPE fluorophore via an amide linkage to construct the fluorescent probe TPEARARG. The uncombined TPEARARG emit weak fluorescence due to the bond rotation. Upon interaction with the arginase, the arginine could enter in the ectodomain of enzyme, resulting in the rotation restriction of TPE, which leading to about 6-fold fluorescence increase at 450 nm (**Figure 1A** ).

The detailed synthesis route and methods of TPEARARG were described in the supporting information. The structure of TPEARARG was characterized with <sup>1</sup>H NMR, <sup>13</sup>C NMR, and HRMS in the supporting information. The optical characterizations of TPEARARG were examined in detail. Firstly, the AIE performances of TPEARARG in various MeOH-H<sub>2</sub>O mixture were tested. As shown in Figure 1B, TPEARARG was weakly fluorescent in MeOH because of the single molecular motion process of TPE. However, its fluorescence intensity enhanced greatly when the water fractions increased due to the formation of depositing aggregates. Moreover, the influence of viscosity on the AIE process was also measured. With the increasing of viscosity, fluorescence emission of TPEARARG enhancement was observed resulted from the rotation restriction of TPE (Figure 1C). These data prove that we have successfully synthesized the TPEARARG with outstanding AIE performances.

Next, the recognition performances of TPEARARG toward arginase were examined. As shown in the Figure 1D and E, upon interaction with sequential dosing of arginase, the fluorescence emission of TPEARARG enhanced swiftly and gradually, which showed a linear manner ( $R^2=0.99$ ). The limit of detection (LOD) was calculated as 0.04 U/mL. The selectivity of TPEARARG to arginase and other proteases was further verified. As revealed in Figure 1F, TPEARARG emitted low fluorescence when incubated with trypsin and other proteases than that with arginase. Moreover, widespread bioactive molecules like reactive oxygen species (ROS), metal ions and amino acids exhibit minimal interferences to the fluorescence of TPEARARG (Figure 1G). The above experimental results show that TPEARARG perform excellent sensitivity and selectivity toward arginase.

Then, the fluorescence responses of TPEARARG to arginase in the PBS from pH 6.0 to pH 8.5 were further tested. Results indicated TPEARARG's great photostability (Figure S1). The cytotoxicity and in vivo toxicity of TPEARARG were measured. As shown in the Figure S2, TPEARARG exhibited weak toxicity on cell proliferation and growth and organ development in mice. Hemolysis test in Figure S3 showed that TPEARARG possessed minimal hemolytic activity (<3%) at tested concentrations (1  $\mu$ M ~ 1 mM). These above experimental results demonstrate that TPEARARG has great potential for biological applications.

### 2.2. Characterizing the binding mode of TPEARARG to arginase

Encouraged by the superior properties of TPEARARG, molecular dynamics (MD) simulations were implemented to confirm the recognition mechanism. Arginase (PDB: 2CEV) was favourably docked into TPEARARG (Figure 2A). Then a 10 ns MD simulation was performed based on Amber99SB force field using Gromacs 2018.4

software. Results exhibited that TPEARARG molecules mainly bound in the cavity consisting of Asp126, Asn128, Ser133, Pro134, His139, Gly140, Ser176, Leu177, Asp178, Glu181, Thr240, and Glu271. The N atoms on the TPEARARG form six hydrogen bonding interactions with Asp126, His139, Asp178, Thr240 and Glu271 in the protein, respectively (Figure 2B). And the benzene ring in the TPEARARG molecule formed strong hydrophobic interactions with the hydrophobic amino acids (Asn128, Ser133, Pro134, Gly140, Ser176, Leu177, Glu181) around the pocket, which further enhanced the affinity between the TPEARARG and arginase (Figure 2C and D). Root mean square deviation (RMSD) revealed that the average number of hydrogen bonds formed between arginase and TPEARARG was  $4.960 \pm 0.732$  (Figure S4). Accordingly, the interaction between arginase and TPEARARG is stable, leading to an obverse fluorescence emission of TPEARARG towards arginase.

### 2.3. Biological application of TPEARARG at the cellular level

Afterward, due to the outstanding detection performances of TPEARARG toward arginase, its biological applications were investigated in living cells in detail. Research works reported that arginase was high expressed in the M2 macrophages<sup>[6a, 6b]</sup>. Thus, the RAW 264.7 cells were stimulated into M1 or M2 type using IFN- $\gamma$ /LPS or IL-4, respectively. The RAW 264.7 cells treated with PBS (pH=7.2) and BEC (An arginase inhibitor) were set as the control groups. Then, the cells were incubated with 1  $\mu$ M TPEARARG and imaged under laser scanning confocal microscope. Compared to the undifferentiated RAW 264.7 and M1 macrophage, the M2 macrophage displayed over 20-fold fluorescence intensity enhancement (Figure 3A and B). In addition, when the arginase was inhibited by BEC, the cellular fluorescence intensity decreased significantly. These results suggest that TPEARARG possess splendid potential in the detection of cellular arginase. To further explore the dynamic detection capability of TPEARARG, we applied the TPEARARG in M2 macrophages with sequential levels of arginase. M2 macrophages were pretreated with BEC for incremental time to obtain reduced expressions of arginase (Figure S5). Then, the TPEARARG was used to observe the variation of cellular arginase. As displayed in Figure 3C and D, with the incubation time increased, the cellular fluorescence intensity decreased gradually. These results confirm that our established imaging method hold great potential in the dynamic detection of cellular arginase.

### 2.4. Observing the activation of CAFs induced by the arginase

Given the overproduction of arginase could increase the metabolism of proline thus induced the ECM deposition in the tissue<sup>[8b, 10]</sup>. We supposed that the overproduction of arginase-induced proline in the TAMs would promote the activation of hepatic stellate cells (HSCs) to differentiate into CAFs, which further aggravated the immune evasion of HCC (Figure 4A). To verify our hypothesis, the proline concentrations in cell culture media with different levels of arginase were examined. As indicated in the Figure 4B, M2 macrophages secreted more proline than M1 macrophages, and the contents of proline decreased when the arginase was inhibited. Further, the proline concentrations depended on the expression of arginase (Figure 4C). These results suggest that the arginase profoundly impacted the produce of proline. Inspired by the above results, we further investigated whether the overproduced proline of TAMs could promote the activation of HSCs. LX-2 cells, a HSCs cell line, were incubated with DMEM (Control), DMEM from M2 macrophage, 10  $\mu$ g/mL proline, 10  $\mu$ g/mL aspartate, and 10  $\mu$ g/mL cysteine, respectively. And the activation maker FAP was imaged using our established probe Cy-FAP. Interestingly, compared to the cells treated with aspartate or cysteine, LX-2 cells incubated with proline exhibited nearly 9-fold enhancement of fluorescence intensity (Figure 4D and E). Similarly, LX-2 cells co-cultured with medium extracted from M2 macrophages showed over 6-fold intensity increase compared with the control, aspartate or cysteine group. When the arginase increases, the activation degree of CAFs was deeper as the fluorescence of Cy-FAP got brighter. These results indicate that elevated proline produced by the M2 macrophage is responsible for the activation of CAFs.

To further prove the contribution of arginase in inducing immune evasion which was mediated by CAFs activation, we measured the PD-L1, IFN- $\gamma$  and IL-10 in each cell group. Experimental data revealed that the expression of PD-L1, IFN- $\gamma$  and IL-10 in LX-2 cells that co-cultured with M2 macrophages raised when compared with the LX-2 cells or M2 macrophages (Figure S6). The above experimental results reveal that M2 macrophages can stimulate the differentiation of HSCs into CAFs by arginase-induced proline secretion,

thereby promoting the immune evasion of HCC.

## 2.5. Activation of HSCs by arginase in mice

To further investigate the mechanism by which arginase promoted immune evasion of HCC cells, we imaged the changes of CAFs in mice with different levels of arginase expression. An orthotopic mouse model of HCC was constructed. The expression of arginase in mice was stimulated using LPS and inhibited by BEC. Subsequently, the mice were incubated with TPEAR and Cy-FAP to imaging the changes of arginase and CAFs. The results showed that the fluorescence intensity of arginase in tumor tissues of mice stimulated with LPS was significantly higher compared to the normal or HCC group. Nevertheless, the fluorescence intensity in mice decreased after inhibition of arginase with BEC (Figure 5A). TPEAR was adequate for monitoring changes of arginase in living mice. In addition, when the content of arginase in mouse tumors was increased, the CAFs exhibited subsequently enhanced activation levels. When arginase was inhibited by the inhibitor, the amount of CAFs then decreased.

To further investigate the immune evasion caused by arginase change, we examined immune evasion related markers in each experimental group. The results exhibited that when the arginase increased, the number of CAFs also increased, which in turn led to the increase of immune evasion-promoting marker CTLA-4 (Figure 5B, Figure S7). Up-regulation of PD-L1, a widely recognized immunosuppressive factor, was also appeared in the HCC mice that arginase was high expressed (Figure 5C). Cytokines IL-10 that reported to contributed to the immunosuppressive effect exhibited up-regulation in the HCC mice that arginase was high expressed (Figure 5D). However, when the arginase was inhibited by the administration of BEC, these immunosuppressive factors were down-regulated, suggesting weaken immune evasion in HCC mice. Furthermore, pro-inflammatory effect like TNF- $\alpha$  and IFN- $\gamma$  revealed down-regulation in the HCC mice that arginase was high expressed (Figure 5E and F). The above experimental data prove that TAMs in vivo stimulate the activation of CAFs via arginase-induced proline production, and then aggravate the immune evasion of HCC.

## 2.6. Signaling pathway underlying the arginase-mediated immune evasion

Ultimately, we determined genes and pathways associated with arginase-induced immune evasion. Mouse models of orthotopic HCC were constructed and treated with LPS as an arginase agonist, then the mRNA in mouse tumor tissues were tested and analyzed. As shown in Figure 6A, the expression of *Oat*, *Scd2*, *Spp1*, and *Preli2* genes related to arginine metabolism, lipid metabolism, and ECM production were elevated in the mice with high arginase expression, indicating elevated activation of HSCs in the tumor tissues of mice with high arginase expression. Further, genes with enhanced immune evasion functions, such as *Map2k6* and *Adipor2*, were highly expressed when the arginase was highly expressed. Our previous work found JAK2-STAT3 signaling pathway through overproduced ROS. Here, we further analyzed the expression of signaling pathways associated with immune evasion in HCC mice. The IL-2-JAK2-STAT signaling pathway associated with oxidative stress was up-regulated when arginase was highly expressed (Figure 6B and C). From the above experimental results, we conclude a new mechanism of arginase promoting immune evasion from HCC: TAMs stimulate the activation of HSCs in the liver to disintegrate into CAFs through high expression of arginase, which in turn promote immune evasion if HCC by interfering with the JAK-STAT signaling pathway through the secretion of excessive ROS.

## 3. Discussion

Previous studies have shown that the interactions of CAFs and TAMs deepened their heterogeneity and promote the development of immune evasion towards a more complex scenario of TME<sup>[7b, 15]</sup>. Investigations have indicated that TAMs can induce the activation of CAFs via cytokine secretion<sup>[7a]</sup>. However, the underlying mechanisms are unclear. Given that the interaction is based on the interaction between active molecules among the CAFs and TAMs, arginase, an immunoregulatory enzyme of TAMs, is involved in the ornithine cycle that plays a crucial role in the production of proline<sup>[16]</sup>. Meantime, proline serves as a major substrate for ECM synthesis by CAFs derived from HSCs<sup>[17]</sup>. Thus, in this study, we set sights on exploring the unique roles of arginase during immune evasion. Tracing the change of arginase during the

immune evasion process in the physiological environment would be beneficial to discovery the underlying mechanisms, but still challenging. Thus, we planned to develop an applicative detection strategy for real-time and in-situ tracing of arginase in living cells and in vivo.

Currently, fluorescence imaging technique is a robust approach for the detection of biologically active molecules<sup>[12, 18]</sup>. In this study, we designed and synthesized the first arginase-specific small molecule fluorescent probe, TPEAR, based on AIE principle. The microenvironmental changes after the enzyme identifies the probe molecule could be utilized by AIE principle. The advantage of this strategy lies in the ability to modulate the probe fluorescence independent of the enzyme-specific cut-off reaction. Consequently, we opted to employ the AIE principle in order to design arginase probes that rely on alterations in the microenvironment subsequent to probe identification of the enzyme's active site. TPEAR can provide powerful assistance in the real-time and in-situ measurement of arginase change and distribution in cells and in vivo.

In this work, presented findings suggest that TAMs generate large amounts of proline by up-regulating the expression of arginase. We suspect this, in turn, may triggers the transformation of HSCs into CAFs within the HCC TME, thereby exacerbating the tumor cells' evasion of immune surveillance. Subsequently, experimental results demonstrated that proline could enhance the fluorescence intensity of Cy-FAP in CAFs, meaning an increased activation of CAFs. By combining the two imaging probes, the interaction between arginase expression in TAMs and the activation process of CAFs was observed for the first time. Proline secreted by TAMs could cause an increased activation of CAFs, while promoting CAFs to secrete more bioactive molecules with immunosuppressive functions. To this point, we find that TAMs produce large amounts of proline through high expression of arginase, which in turn stimulates CAFs to deepen the degree of immune evasion.

Furthermore, the detailed molecular mechanism of the process was explored. The JAK-STAT signaling pathway was found to be an important mechanism deeply involved in immune evasion from cancer cells in previous work<sup>[19]</sup>. Encouragingly, the results revealed that arginase mediated the down-regulation of JAK-STAT signaling pathway in CAFs via secretion of proline by TAMs. Then, increased secretion of PD-L1 and enhanced immune evasion of HCC were showed, which validated our previous conclusion.

In summary, by utilizing a new arginase-specific probe TPEAR and our established CAFs-specific probe Cy-FAP, we presented a dual imaging strategy for simultaneous observation of TAMs and CAFs. We applied this method in cells and in vivo to measure the changes of arginase and CAFs activation. Subsequently, using our established CAFs-specific imaging platform, we further explored the detailed molecular mechanism of arginase promoting immune evasion in HCC. Results showed that TAMs promoted the activation of CAFs by elevating proline levels through high expression of arginase, and CAFs deepened TAMs-induced immune evasion of HCC by secreting immunosuppressive active molecules. This approach we developed will provide a powerful tool for the study of arginase. Results has revealed a novel role played by arginase during immune evasion, which provided a new therapeutic target for HCC.

## 4. Experimental Section

### 4.1. Materials and Reagents

All chemical reagents were purchased from Shanghai xianding biotechnology co., LTD. Analytical grade solvents were used without further purification. Mouse PD-L1 and TNF- $\alpha$  ELISA kits were purchased from Absin Bioscience Inc. Raw264.7, LX-2 cells and all supplies for cell culture were purchased from Boster Biological Technology co. ltd.

### 4.2. Instruments

UV-2600 UV-visible spectrophotometer (Shimadzu, Japan) was utilized to analyze absorption spectra. The F-4600 HITACHI fluorescence spectrophotometer was used to detect the fluorescence spectra. Utilizing the Bruker maXis ultra-high resolution-TOF MS equipment, mass spectra were identified. Using Bruker NMR spectrometers, <sup>1</sup>H NMR spectra were measured at 400 MHz, while <sup>3</sup>C NMR spectra were recorded

at 100 MHz. Using a Leica TCS SP8 confocal laser scanning microscope, fluorescence imaging of cells was performed. Using the Perkinelmer IVIS Lumina III, in vivo NIR imaging of mice was measured.

### 4.3. Synthesis of TPEARG

The synthetic route was displayed in Figure S8. 347 mg, 1 mmol 1-(4-Aminophenyl)-1,2,2-triphenylethene and 649 mg, 1 mmol N $\alpha$ -Fmoc-N $\omega$ -(2,2,4,6,7-pentamethyldihydrobenzofuran-5-sulfonyl)-L-arginine was dissolved to 10 mL tetrahydrofuran (THF), then stirred in room temperature under nitrogen protection for 10 min. 277 mg, 1 mmol 4-(4,6-Dimethoxy-1,3,5-triazin-2-yl)-4-methylmorpholinium chloride was added into the solution and reacted for another 3 h. Then, the THF was removed by vacuum distillation. Then, the solid was added into 5 mL piperidine and 5 mL dichloromethane (DCM), then stirred in room temperature under nitrogen protection for 2 h. The solvent was removed by vacuum distillation. After that, 1 mL trifluoroacetic acid and 9 mL DCM was added to the solid mixture and stirred for 1 h. TPEARG was purified by chromatography on silica gel with dichloromethane/methanol (10:1) as faint yellow powder (9%). HRMS (ESI):  $m/z$  calcd for C<sub>32</sub>H<sub>33</sub>N<sub>5</sub>O [M]<sup>+</sup> 504.2757, found in 504.2686. <sup>1</sup>H NMR (400 MHz, Methanol-*d*<sub>4</sub>)  $\delta$  7.77 (d,  $J$  = 7.5 Hz, 1H), 7.63 (t,  $J$  = 7.3 Hz, 1H), 7.30 (ddd,  $J$  = 24.7, 16.3, 6.3 Hz, 4H), 7.07 (s, 4H), 7.00 (d,  $J$  = 12.2 Hz, 2H), 6.91 (s, 0H), 4.38 (d,  $J$  = 6.7 Hz, 1H), 4.18 (t,  $J$  = 8.8 Hz, 1H), 3.99 (s, 1H), 2.93 (s, 1H), 2.51 (d,  $J$  = 24.9 Hz, 3H), 2.02 (s, 2H), 1.40 (s, 3H), 0.88 (d,  $J$  = 4.3 Hz, 1H). <sup>13</sup>C NMR (101 MHz, CDCl<sub>3</sub>)  $\delta$  175.79, 170.45, 166.45, 161.24, 152.52, 145.08, 142.69, 140.92, 139.86, 133.39, 128.98, 128.71, 126.99, 121.71, 116.38, 110.92, 105.08, 64.55, 60.68, 49.63, 47.12, 39.51, 34.88, 29.54, 28.30, 28.10, 21.67, 18.16, 12.71, 11.58, 0.75, 0.37.

### 4.4. Calculation of the LOD

The detection limit was calculated employing the following formula: Detection limit =  $3\sigma/k$ , where  $\sigma$  is the standard deviation of blank measurement,  $k$  is the slope between the fluorescence intensity and the concentration of arginase.

### 4.5. Cell Culture

Dulbecco's Modified Eagle's Medium (DMEM) supplemented with 10% heat-inactivated fetal bovine serum and 1% penicillin and streptomycin was used to culture Raw 264.7 and LX-2 cells. Cells were grown at 37 °C in a humidified environment of 5% CO<sub>2</sub>. Medium replacements were made one or two days. LX-2 cells were collected using pancreatin and Raw 264.7 cells were collected by DMEM washing.

### 4.6. Cytotoxicity Assays

Raw 264.7 cells were seeded in two 96-well plates at a concentration of  $1 \times 10^5$  and cultured for 12 h. In one 96-well plates, cells were cultured with 0, 500 nM, 50  $\mu$ M, 100  $\mu$ M, 200  $\mu$ M, 500  $\mu$ M TPEARG for 12 h. The medium volume of every well was 100  $\mu$ L. Then, 10  $\mu$ L CCK-8 solution was added to each well and incubated for another 1 h at 37 °C. After that, the absorbance at 450 nm was detected in a Triturus microplate reader.

### 4.7. In Vivo Toxicity Assays

C57BL/6J mice (male, 4-6 weeks) were housed in a pathogen-free, temperature controlled facility with 12-hour light/dark cycles. Animals received food and water ad libitum.

Mice were divided into two groups (6 mice per group). The mice in control group were given 200  $\mu$ L PBS (pH=7.4) solution via intravenous injection per day for 7 days. The mice in experimental group were given 200  $\mu$ L 200  $\mu$ M TPEARG PBS solution (pH=7.4) via intravenous injection per day for 7 days. Their body weights were recorded every day. At the end of the experiment, major organs of heart, liver, spleen, lung and kidney in mice of each group were obtained and stained with hematoxylin and eosin (H&E) to assess toxicity.

### 4.8. Establishment of Orthotopic Mouse Model of HCC

C57BL/6J mice (male, 4-6 weeks) were subcutaneous injected with  $1 \times 10^7$  HEPA 1-6 cells at the armpit of the right anterior limb. After 2-3 weeks, the mice were sacrificed by anaesthetic overdose. The grown tumors were separated and cut into small pieces (1-2 mm<sup>3</sup>). Then, these pieces of tumor were transplanted to the

livers of other healthy mice through surgical operation. To preserve the activity of tumor pieces, surgical operation time should be completed within 30 minutes.

#### **4.9. Fluorescence Imaging of Cells In Vitro**

RAW 264.7 and LX-2 cells were seeded on the round coverslips in 6-well plates and then treated cells with different reagents. For arginase imaging, cells incubated with 100  $\mu$ L 1  $\mu$ M TPEARARG PBS solution (1% DMF) for 30 minutes. Then the cells were washed with PBS 3 times, and imaged under the confocal laser scanning microscope with a blue channel ( $\lambda_{\text{ex}}=405$  nm (intensity=5%),  $\lambda_{\text{em}}=410$  nm- 480 nm). For FAP imaging, cells were incubated with 100  $\mu$ L 20  $\mu$ M Cy-FAP PBS solution for 30 minutes. Then the cells were washed with PBS 3 times, and imaged under the confocal laser scanning microscope with a red channel ( $\lambda_{\text{ex}}=633$  nm (intensity=6%),  $\lambda_{\text{em}}=700$  nm- 780 nm) for Cy-FAP.

#### **4.10. Fluorescence Imaging of Mice Tissue**

The control group sham surgery group. Orthotopic mouse models of HCC were randomly divided into several groups (n=5). Mice was injected with 50  $\mu$ L 10  $\mu$ M TPEARARG PBS solution (1% DMF) and 50  $\mu$ L 20  $\mu$ M Cy-FAP PBS solution for 30 minutes via tail veins, respectively. Then liver tissues of each mouse were sliced using Leica CM1950. Fluorescence imaging of mice tissues were carried out using laser scanning microscope with a blue channel ( $\lambda_{\text{ex}}=405$  nm (intensity=8%),  $\lambda_{\text{em}}=410$  nm- 480 nm) for TPEARARG and a red channel ( $\lambda_{\text{ex}}=633$  nm (intensity=10%),  $\lambda_{\text{em}}=700$  nm- 780 nm) for Cy-FAP.

#### **4.11. In Vivo Cytokine Analysis**

Excised tumor tissues (100 mg) or cells ( $1 \times 10^6$ ) were homogenized in protease inhibitor-containing protein extraction buffers (1 mL). IL-10, IFN- $\gamma$ , PD-L1 and TNF- $\alpha$  were tested using ELISA kits in accordance with the manufacturer's recommendations.

#### **4.12. Western Blotting.**

The following procedures were used to lyse the cells: Cold PBS was used to wash the cells for three times. Cells were then gathered using an enzyme-free dissociation buffer, and then lysed using an ice-cold RIPA buffer contained phosphatase and protease inhibitors. Lysates were performed on 10% SDS-Tris glycine gels for 2 h and then transferred to PVDF membranes (45  $\mu$ m) for 1 h. The PVDF membranes were blocked using 5% w/v skim milk for 2h. The primary antibody was then incubated on the membranes overnight at 4  $^{\circ}$ C. Secondary antibody was incubated for 2h at 4  $^{\circ}$ C. Pierce ECL Western Blotting Substrate was used to view the signals, and ImageJ was used to quantify the signals. GAPDH was measured as a control.

#### **4.13. Statistical Analysis**

Values in this study were expressed as mean  $\pm$  standard deviation (SD). Differences between two groups were analyzed by using two-tailed, unpaired Student's t test. P value < 0.05 was considered statistically significant.

#### **Ethics Statement**

All animals received humane care according to the criteria outlined in the "Guide for the Care and Use of Laboratory Animals". Animal protocols were approved by the Ethics Committee of Shandong Normal University (AEECDNU2022022).

#### **Conflict of Interests**

The authors declare no conflict of interests.

#### **Data Availability Statement**

The data that support the findings of this study are available from the corresponding author upon reasonable request.

#### **Supporting Information**

Supporting Information is available from the Wiley Online Library or from the author.

#### Acknowledgements

This work was supported by the National Natural Science Foundation of China (22134004, 22074083, 21927811), the Key Research and Development Program of Shandong Province (2018YFJH0502), Natural Science Foundation of Shandong Province of China (ZR2020ZD17, ZR2023YQ016, ZR2021QB042), Local Science and Technology Development Fund Guided by the Central Government of Shandong Province (YDZX2022012), and the Major Science and Technology Innovation Project of Shandong Province (2021ZD-SYS09).

Received: ((will be filled in by the editorial staff)) Revised: ((will be filled in by the editorial staff)) Published online: ((will be filled in by the editorial staff))

#### References

- [1] E. N. Arner, J. C. Rathmell, *Cancer Cell* **2023** ,41 , 421-433.
- [2] R. Donne, A. Lujambio, *Hepatology* **2023** ,77 , 1773-1796.
- [3] aJ. M. Llovet, F. Castet, M. Heikenwalder, M. K. Maini, V. Mazzaferro, D. J. Pinato, E. Pikarsky, A. X. Zhu, R. S. Finn, *Nat Rev Clin Oncol* **2022** , 19 , 151-172; bJ. Puleo, K. Polyak, *Biochim Biophys Acta Rev Cancer* **2022** , 1877 , 188671.
- [4] K. E. de Visser, J. A. Joyce, *Cancer Cell* **2023** ,41 , 374-403.
- [5] I. Kaymak, K. S. Williams, J. R. Cantor, R. G. Jones, *Cancer cell* **2021** , 39 , 28-37.
- [6] aL. Cassetta, J. W. Pollard, *Nat Rev Cancer* **2023** , 23 , 238-257; bN. Cox, M. Pokrovskii, R. Vicario, F. Geissmann, *Annu Rev Immunol* **2021** , 39 , 313-344; cD. G. DeNardo, B. Ruffell, *Nat Rev Immunol* **2019** ,19 , 369-382.
- [7] aX. Mao, J. Xu, W. Wang, C. Liang, J. Hua, J. Liu, B. Zhang, Q. Meng, X. Yu, S. Shi, *Mol Cancer* **2021** , 20 , 131; bH. Raskov, A. Orhan, S. Gaggari, I. Gogenur, *Front Oncol* **2021** , 11 , 668731.
- [8] aD. W. Christianson, *Accounts of chemical research* **2005** , 38 , 191-201; bA. Matos, M. Carvalho, M. Bicho, R. Ribeiro, *Nutrients* **2021** , 13 .
- [9] S. Cane, R. M. Barouni, M. Fabbi, J. Cuzzo, G. Fracasso, A. Adamo, S. Ugel, R. Trovato, F. De Sanctis, M. Giacca, R. Lawlor, A. Scarpa, B. Rusev, G. Lionetto, S. Paiella, R. Salvia, C. Bassi, S. Mandruzzato, S. Ferrini, V. Bronte, *Sci Transl Med* **2023** ,15 .
- [10] M. Tsoumakidou, *Nat Rev Cancer* **2023** , 23 , 258-269.
- [11] aQ. T. Chen, Z. Y. Zhang, Q. L. Huang, H. Z. Chen, W. B. Hong, T. Lin, W. X. Zhao, X. M. Wang, C. Y. Ju, L. Z. Wu, Y. Y. Huang, P. P. Hou, W. J. Wang, D. Zhou, X. Deng, Q. Wu, *Nat Metab* **2022** , 4 , 1306-1321; bC. R. Gandhi, *J Hepatol* **2017** , 67 , 1104-1105.
- [12] aY. Geng, Z. Wang, J. Zhou, M. Zhu, J. Liu, T. D. James, *Chem Soc Rev* **2023** , 52 , 3873-3926; bL. Wu, A. C. Sedgwick, X. Sun, S. D. Bull, X. P. He, T. D. James, *Acc Chem Res* **2019** , 52 , 2582-2597; cH. Shen, F. Sun, X. Zhu, J. Zhang, X. Ou, J. Zhang, C. Xu, H. H. Y. Sung, I. D. Williams, S. Chen, R. T. K. Kwok, J. W. Y. Lam, J. Sun, F. Zhang, B. Z. Tang, *J Am Chem Soc* **2022** , 144 , 15391-15402.
- [13] K. C. Chong, F. Hu, B. Liu, *Materials Chemistry Frontiers* **2019** , 3 , 12-24.
- [14] T. Zang, Y. Xie, S. Su, F. Liu, Q. Chen, J. Jing, R. Zhang, G. Niu, X. Zhang, *Angew Chem Int Ed Engl* **2020** , 59 , 10003-10007.
- [15] P. Yang, H. Qin, Y. Li, A. Xiao, E. Zheng, H. Zeng, C. Su, X. Luo, Q. Lu, M. Liao, L. Zhao, L. Wei, Z. Varghese, J. F. Moorhead, Y. Chen, X. Z. Ruan, *Nat Commun* **2022** , 13 , 5782.





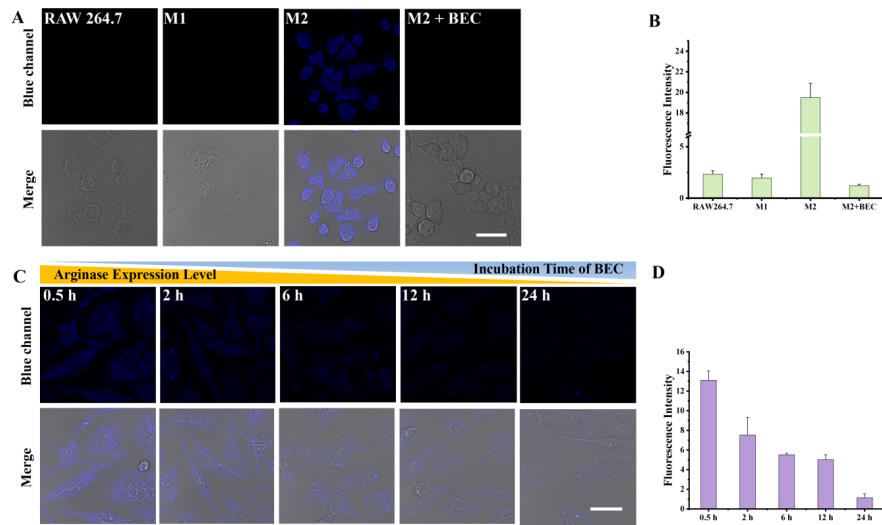


**Figure 3. Biological application of TPEARG in living cells.** (A) 1  $\mu$ M TPEARG was added in the RAW264.7 cells, M1 macrophages, M2 macrophages, and M2 macrophages pretreated with BEC (An arginase inhibitor), and imaged under the excitation of 400 nm. (B) Fluorescence intensity output of each group in Figure 3A. (C) Dynamic imaging detection of arginase using TPEARG in M2 macrophages pretreated with BEC for incremental time. (D) Fluorescence intensity output of Figure 3C. The data are expressed as mean  $\pm$  SD.

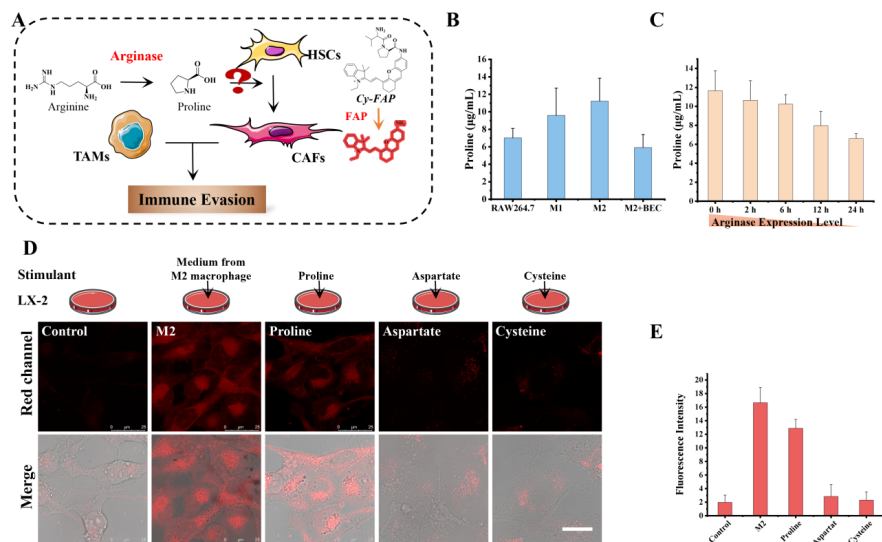


**Figure 4. Activation of hepatic stellate cells (HSCs).**(A) Hypothesis of the arginase in the TAM inducing the activation of HSCs to differentiate into cancer-associated fibroblasts (CAFs), which further aggravating the immune evasion. (B) Proline production by RAW 264.7 (Inactivated), M1 macrophage, M2 macrophage, and M2 macrophage incubated with BEC. (C) Measurement of proline secreted by M2 macrophage incubated with BEC for incremental time. (D) LX-2 cells, a HSCs cell line were incubated with DMEM (Control), DMEM from M2 macrophage, DMEM with 10  $\mu$ g/mL proline, DMEM with 10  $\mu$ g/mL aspartate, and 10  $\mu$ g/mL cysteine, respectively. Then, the FAP in LX-2, a marker of CAFs, were imaged using 10  $\mu$ M/mL Cy-FAP. (E) Fluorescence intensity output of Figure 4D. The data are expressed as mean  $\pm$  SD. n = 3. Scale bar= 25  $\mu$ m.

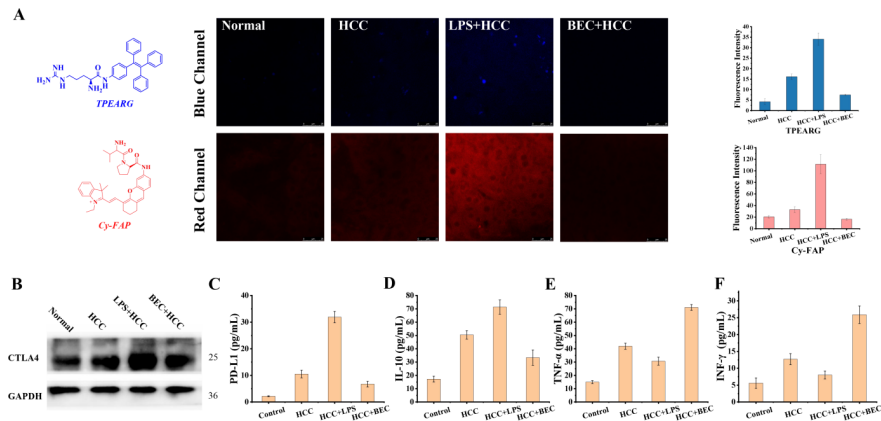


**Figure 5. Activation of HSCs by arginase in mice.** (A) Cy-FAP and TPEARNG were applied in the normal mice (Control) and orthotopic mouse models of HCC treated with LPS (Arginase agonist) and BEC (Arginase inhibitor). (B) Western blot of CTLA4 in each mouse group. ELISA Kit test of the expressions of immune evasion markers PD-L1 (C), TNF- $\alpha$ (D), IL-10 (E) and IFN- $\gamma$  (F). The data are expressed as mean  $\pm$  SD. n = 3. Scale bar= 25  $\mu$ m.

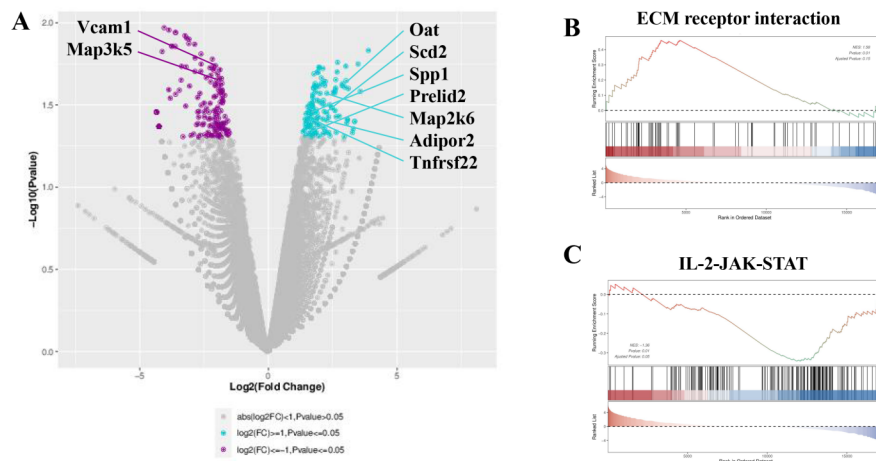


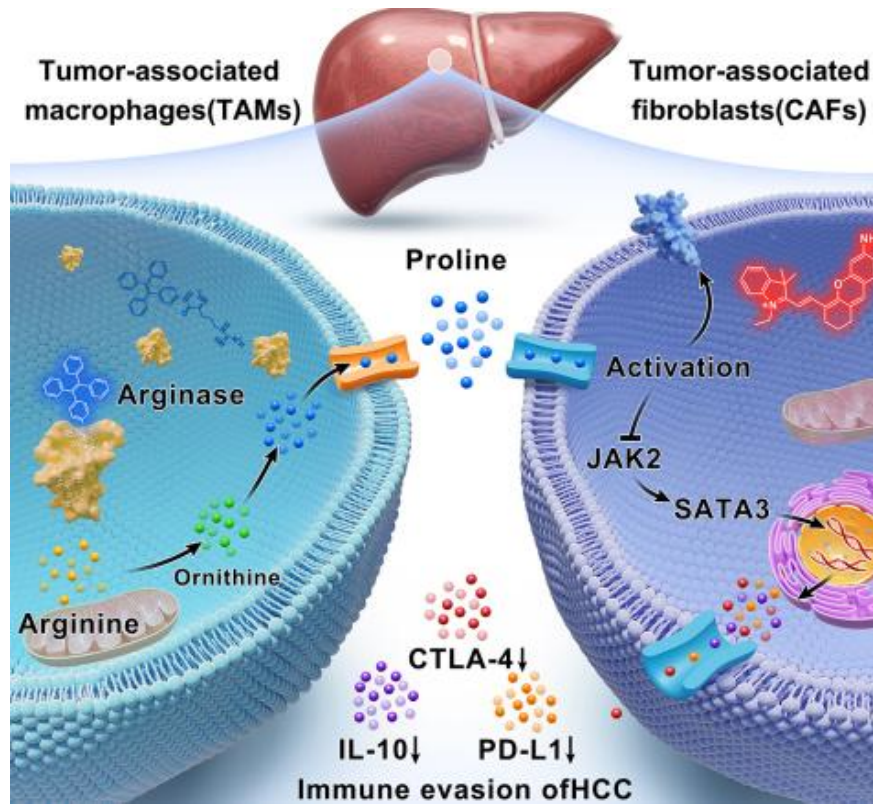
**Figure 6. Genes and pathways analysis in mice with arginase high expression.** (A) Gene set enrichment analysis (GSEA) comparing gene-expression data from mouse tumor tissue and that treated with LPS. GSEA of the Hallmark ‘ECM receptor interaction’ (B) and ‘IL-2-JAK-STAT Signaling’ (C) pathway in mice tumor tissue.

Arginase is a key enzyme in tumor-associated macrophages (TAMs) and plays an important role in TAM-mediated immune evasion, but its in-situ variation and relevant mechanism are unclear. In this work, dynamic changing of arginase in TAMs is observed during immune evasion of HCC. Results reveal that arginase initiates proline production and then activates tumor-associated fibroblasts, enhancing immune evasion in HCC.

**Keywords:** Fluorescent probe, Arginase, Tumor-associated macrophages, Immune evasion, Tumor-associated fibroblasts

Chuanchen Wu, Yuantao Mao, Xinru Qi, Xin Wang, Ping Li, \* Wen Zhang and Bo Tang \*

**Title: Tracking interactions between TAMs and CAFs mediated by arginase-induced proline production during immune evasion of HCC**



Supporting Information

**Tracking interactions between TAMs and CAFs mediated by arginase-induced proline production during immune evasion of HCC**

Chuanchen Wu, Yuantao Mao, Xinru Qi, Xin Wang, Ping Li, \* Wen Zhang and Bo Tang \*

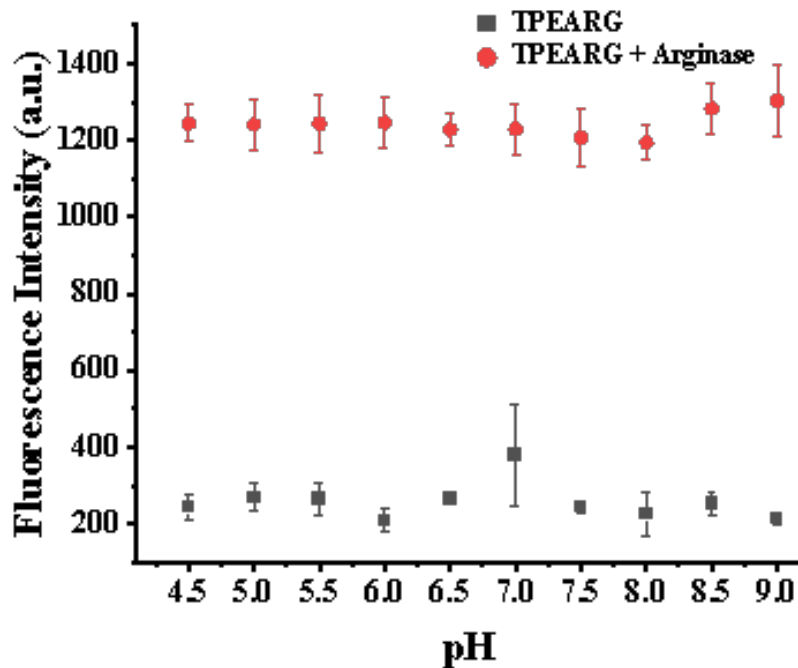


**Figure S1** Fluorescence enhancement of TPEARG (1  $\mu\text{M}$ ) with and without arginase (0.8 U/mL in PBS) in different pH. The data are expressed as the mean  $\pm$  SD. Error bars represent standard deviations of three separate measurements.

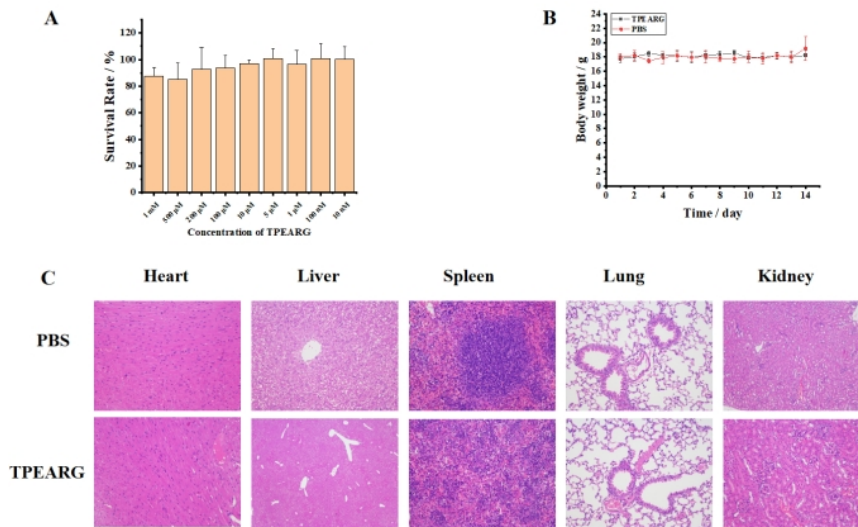


**Figure S2** Biocompatibility of TPEARG. (A) RAW264.7 cells were cultured with 500 nM, 50  $\mu\text{M}$ , 100  $\mu\text{M}$ , 200  $\mu\text{M}$ , 500  $\mu\text{M}$  TPEARG for 12 h. Then the cell survival rate was tested using CCK8. (B) Body weight changes of mice treated with PBS and 200  $\mu\text{M}$  TPEARG. (C) Hematoxylin and eosin (H&E) staining of major organs of mice treated with PBS and TPEARG. The data are expressed as the mean  $\pm$  SD. Error bars represent standard deviations of three separate measurements.

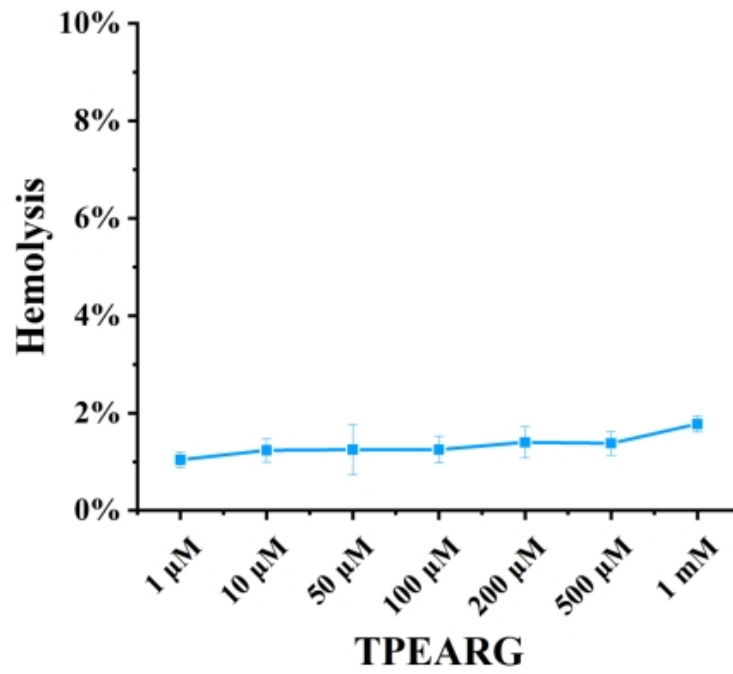


**Figure S3** Hemolysis test of TPEARG from 1 μM to 1 mM.

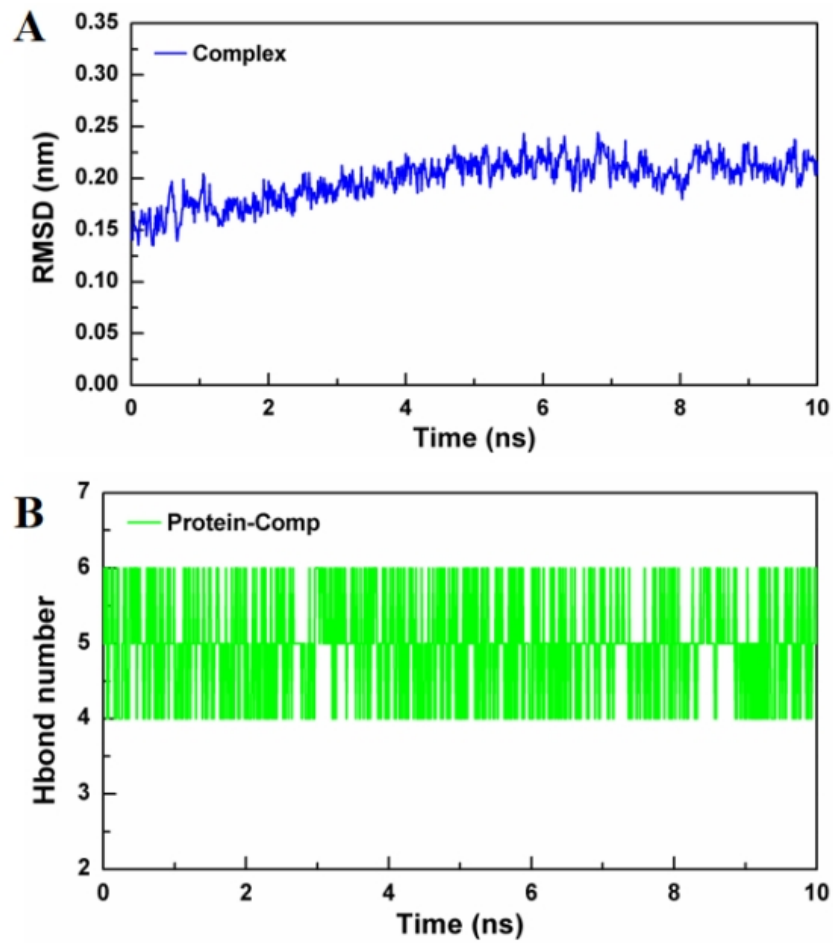


**Figure S4** The root mean square deviation (RMSD) value (A) and the hydrogen bond (B) between TPEAR-G and protein of the complex system changed with simulation time.

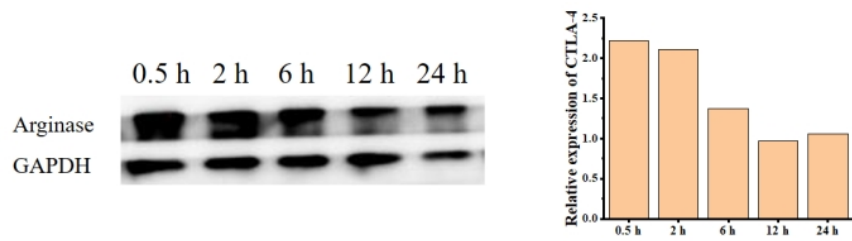


**Figure S5** Arginase expression in M2 macrophages pretreated with BEC for incremental time.

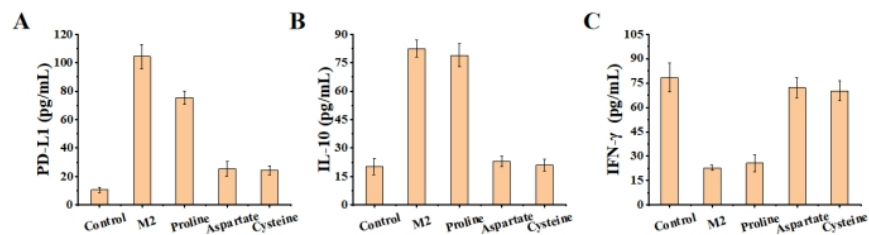


**Figure S6** The expression of PD-L1(A), IFN- $\gamma$ (B) and IL-10(C) in LX-2 cells that co-cultured with DMEM (Control), DMEM from M2 macrophage, 10  $\mu$ g/mL proline, 10  $\mu$ g/mL aspartate, and 10  $\mu$ g/mL cysteine, respectively.

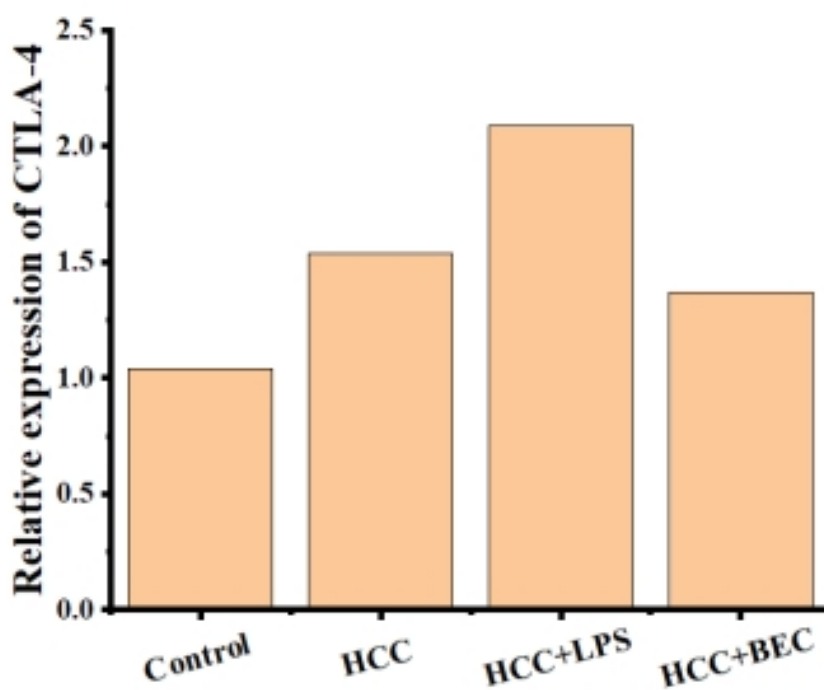


**Figure S7** Data output of Figure 5B.

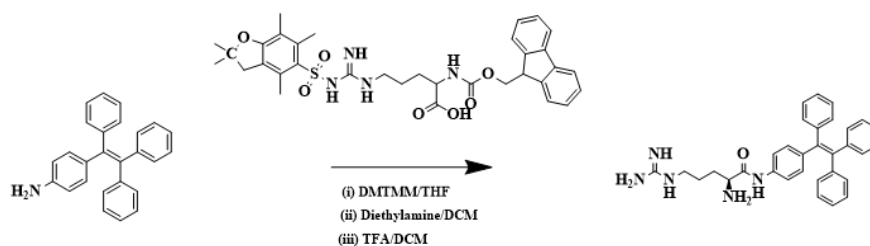
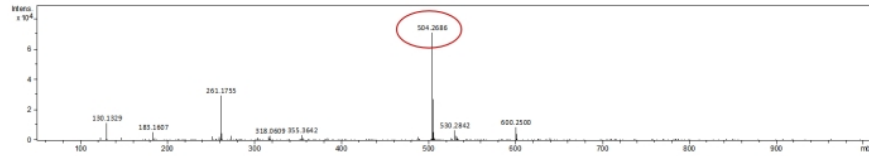
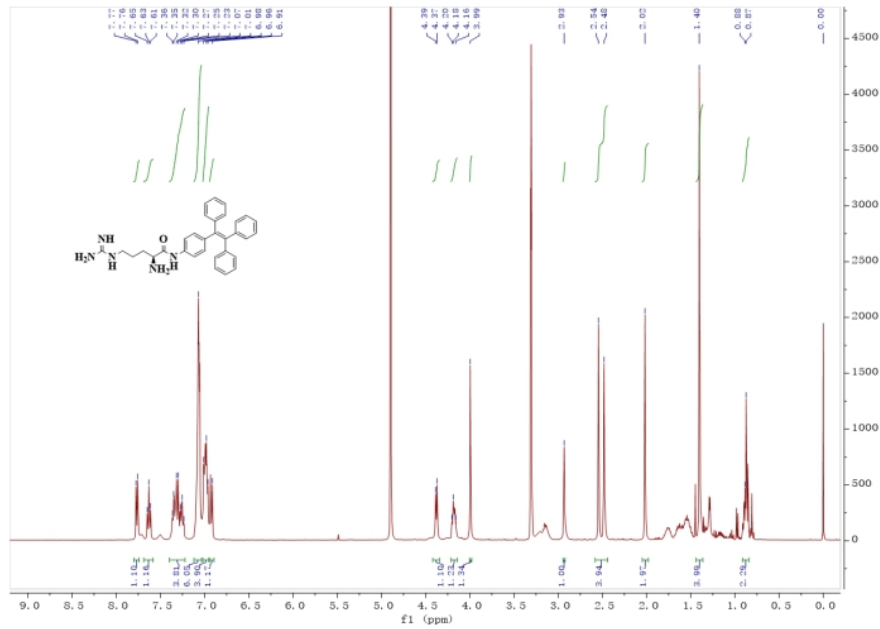


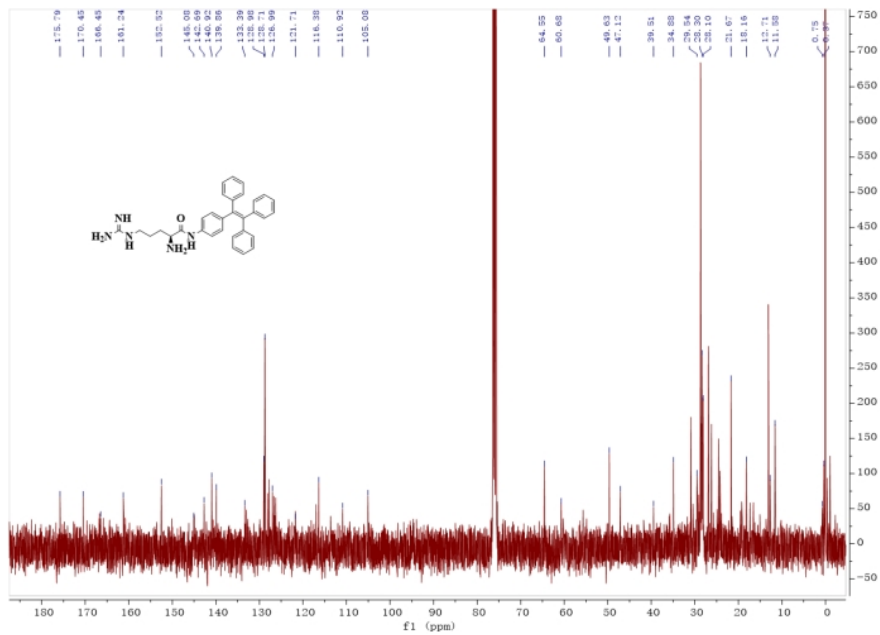
**Figure S8** Synthetic route of TPEARG .



The HRMS(ESI) of TPEARG.



The <sup>1</sup>H NMR spectra of TPEARG.



## The $^{13}\text{C}$ NMR spectra of TPEAR.G.